PROCEEDINGS OF SCIENCE
ONLINE ICRC 2021

Gamma-ray burst observation & gravitational wave event follow-up with CALET on the International Space Station

Yuta Kawakubo[a,*] **on behalf of the CALET Collaboration**
(a complete list of authors can be found at the end of the proceedings)

[a] *Department Physics & Astronomy, Louisiana State University, 202 Nicholson Hall, Baton Rouge, LA 70803, USA*

E-mail: kawakubo1@lsu.edu

The CALorimetric Electron Telescope (CALET) has been observing high-energy cosmic rays and gamma-rays on the International Space Station since October 2015. The CALET gamma-ray burst monitor (CGBM), mounted on CALET to observe prompt emissions of gamma-ray bursts (GRBs) in the hard X-ray and soft gamma-ray band, has been monitoring all-sky with ~ 60 % duty cycle without any problems since October 2015. As of end May 2021, CGBM has detected 254 GRBs, including 31 short GRBs, thanks to the onboard trigger system. The Calorimeter (CAL), the primary instrument of CALET, has also collected gamma-ray data in the energy range from 1 GeV to 10 TeV while maintaining both instruments in good condition. We continue searching for high-energy gamma-rays from GRBs detected by CGBM, and have found two possible gamma-rays from GRBs. As described above, CALET can detect prompt emissions and high energy gamma-ray emission of GRBs. Therefore, we also have actively participated in the follow-up campaign for electromagnetic counterparts of the gravitational wave events observed by LIGO/Virgo since the operation start of the CALET. Although we have found no candidates of electromagnetic counterparts of the gravitational wave events, we have derived upper limits of the high-energy gamma-ray flux for 26 events in the LIGO/Virgo third observation run.

37th International Cosmic Ray Conference (ICRC 2021)
July 12th – 23rd, 2021
Online – Berlin, Germany

*Presenter

PoS(ICRC2021)957

1. Introduction

Gamma-ray bursts (GRB) have been observed by many telescopes in space and on the ground in various wavelengths since the discovery by the Vela satellite [1][2]. In recent years, GRBs, especially short GRBs, have taken on increased importance because a short GRB is a plausible candidate for gravitational wave events' electromagnetic counterparts. *Fermi*-GBM and *INTEGRAL* SPI-ACS detected GRB 170817A in association with binary neutron star merger GW 170817 [4][5]. Since GRB 170817A is the only GRB observed and associated with a gravitational wave event, further detection of GRBs associated with gravitational wave events is essential to understand the association between binary neutron star mergers and short GRBs, and the short GRB itself.

Since the coverage by a single GRB instrument is limited, observing GRBs with multiple instruments increases the validity of the observation and the chance of detecting GRBs associated with gravitational wave events. The CALorimetric Electron Telescope (CALET) is a payload on the International Space Station [7]. CALET consists of the Calorimeter (CAL) and CALET Gamma-ray burst monitor (CGBM). CALET has been monitoring all-sky with X-ray and gamma-rays. In particular, CGBM has been detecting GRBs with a rate of $\sim$ 45 GRBs / year. In this paper, we will present an overview of GRB observations with CALET in five years. Also, we will present a summary of follow-up observations for electromagnetic counterparts of gravitational wave events in the LIGO/Virgo third observation run. Detailed gamma-ray observations of CAL will be presented in different papers in ICRC 2021 [8][9].

2. GRB observation with CALET

In GRB observations with CALET, CGBM is primarily responsible for observing prompt emission of GRBs. CGBM consists of two Hard X-ray Monitors (HXMs) and a Soft Gamma-ray Monitor (SGM) [10][11]. Both HXM and SGM are scintillation detectors that have $LaBr_3$(Ce) and BGO for each. CGBM covers the energy range from 7 keV to 20 MeV thanks to HXM (7 keV - 1 MeV) and SGM (40 keV - 20 MeV). CGBM collects two types of monitor data continuously: Time History (TH) data, which have eight energy channels and are collected every 1/8 s, and Pulse Height (PH) data, which have 512 energy channels, are collected every 4 s. CGBM has an onboard trigger system to detect GRBs and other X-ray/gamma-ray transients. The onboard trigger system calculates the signal-to-noise ratio (SNR) according to (1)

$$\mathrm{SNR} = \frac{N_{\mathrm{tot}} - \frac{N_{\mathrm{BG}}}{\Delta t_{\mathrm{BG}}}\Delta t}{\sqrt{\frac{N_{\mathrm{BG}}}{\Delta t_{\mathrm{BG}}}\Delta t}} \tag{1}$$

where Δt is the integration time of the foreground (1/4 s, 1/2 s, 1 s, and 4 s); Δt_{BG} is integration time of the background (8, 16, 32, 64 s). N_{tot} is integrated counts over Δt in the selected energy range, and N_{BG} is integrated counts over Δt_{BG} in the selected energy range. In the flight operation, trigger thresholds (σ) are selected from 4, 5.5, 7, 8.5, 10, 11, and 13 for each Δt. Δt_{BG} is selected from 8 s, 16 s, 32 s, 64 s and used for all Δt conditions. Δt_{BG} is taken from a time interval before Δt. Since CGBM has three sensors, and there are four Δt conditions, SNRs are calculated every 1/4 s in the twelve trigger conditions in parallel. If any SNRs exceed trigger thresholds, CGBM captures event data that have higher time and energy resolution than those of monitor data. The onboard CGBM buffer is able to store four events. If four triggers occur before downlink, the onboard trigger is disabled until the event data is transferred and deleted from the buffer. Also, the ground analysis server analyzes real-time TH data and sends an alert as a GCN notice when a CGBM onboard trigger occurs. The trigger settings as of May 31, 2021, are shown in Table 1.

Figure 1 shows averaged count rate maps of each CGBM detector. Background count rates due to charged particles highly depend on geomagnetic position. CGBM count rates increase at the high latitude and around the South Atlantic Anomaly (SAA). CGBM high voltages are turned off at high latitude and around the SAA to avoid high count rates and false triggers due to charged particles. As a result, the duty cycle of CGBM is $\sim$ 60 %. Since background count rates vary depending on time, CGBM is triggered by high count rates due to charged particles sometimes, even if the CGBM high voltages are turned off at the high count rate region. Since HXM has a sensitivity to X-ray below 10 keV, bright X-ray sources in the HXM field of view cause increased HXM count rates. Figure 2 shows background spectra observed by each CGBM detector on October 5 in 2015 and April 5 in 2021. CGBM has been collecting X-ray and gamma-rays data without any problem for more than five years since the operation start. All CGBM detectors can see the 511 keV line due to annihilation. Two internal background lines can be seen around 35 keV and 1470 keV in the HXM background spectra [12]. The 2.2 MeV line originating from activation can be seen in the SGM background spectra [13]. These background lines can be used for energy calibration.

At the end of May 2021, CGBM has detected 254 GRBs thanks to the onboard trigger system. The total observation interval is 2066 days, and the GRB detection rate is 44.9 GRBs / year. Figure 3 shows the T_{90} distribution of GRBs detected by CGBM. T_{90} was measured by SGM in the energy range 40 $\sim$ 1000 keV using 'battblocks', which is software for *Swift*-BAT data to measure the duration using the Bayesian block method [14]. Although TH data were used for T_{90} calculation, event data were used if calculated T_{90} was less than 2 s. Since 5 out of 254 GRBs were low significance or not seen in SGM data, 249 GRBs were included in Figure 3. The T_{90} distribution by CGBM is bimodal in logarithmic scale like those by other instruments, and well fitted with two logarithmic normal distributions. The means of the two logarithmic normal distributions were 0.51 s and 16.98 s. The intersection of the two logarithmic normal distributions was 1.44 s. If we classify GRBs by 1.44 s, the number of long bursts and short bursts were 218 and 31, respectively. Also, the five GRBs for which SGM did not measure T_{90} were long GRBs judging from HXM data. Therefore, 12.4 % of GRBs seen by CGBM were short GRBs. Figure 4 shows the GRB position in SGM coordinates with regions obstructed by fixed structures. Since CGBM has no capability of GRB localization, we used GRB positions that were reported to GCN by other GRB instruments [15]. 182 out of 254 GRBs were localized by other GRB instruments and included in Figure 4.

Table 1: Settings for CGBM onboard trigger

	HXM	SGM
Trigger threshold σ	8.5	7.0
Δt_{BG}	16 s	16 s
Energy range	25 $\sim$ 100 keV	50 $\sim$ 300 keV

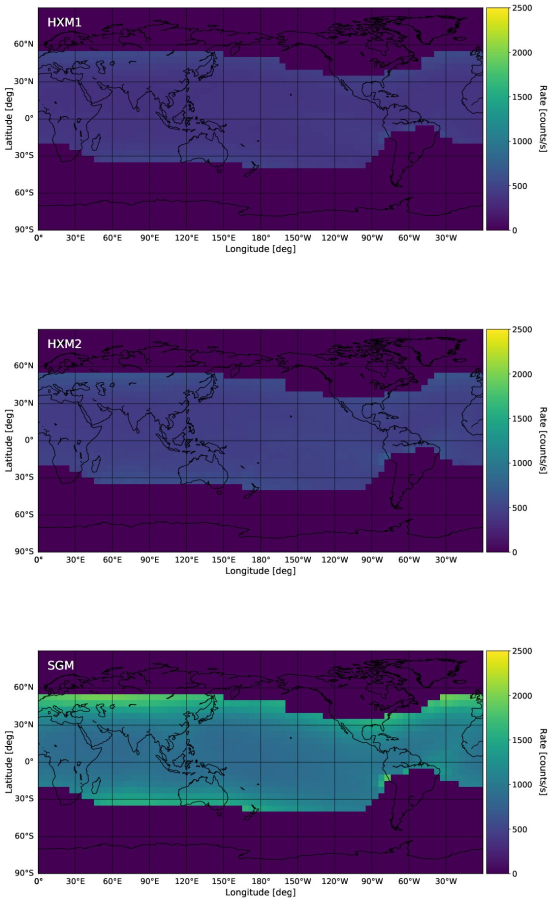

Figure 1: Background count rate maps measured by CGBM. The top, middle, and bottom panels are averaged count rate maps for each geographic position for HXM1, HXM2 and SGM, respectively. The count rates were calculated using PH data for September 2020 and averaged in each 5 deg. pixel.

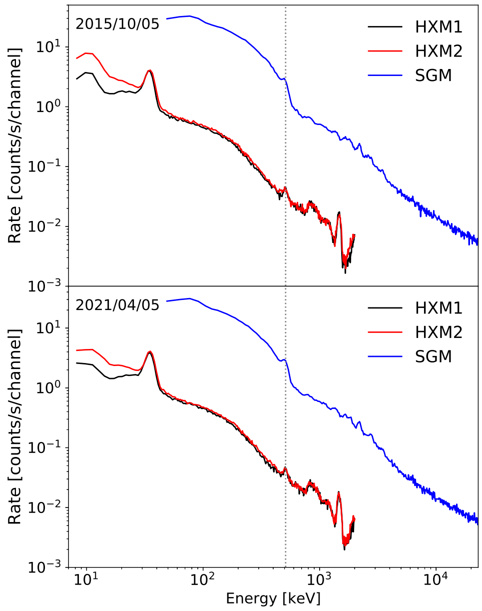

Figure 2: Background spectra of CGBM. The top and bottom panels shows time averaged background spectra for 1000 s on October 5 2015 and April 5 2021. HXM and SGM gains were corrected by the position of 1.4 MeV and 2.2 MeV lines for each. Gray dotted lines show the position of 511 keV.

Since CALET is not a satellite but a payload on the ISS, ISS structures obstruct the CAL and CGBM fields of view. In addition to fixed structures, there are both regularly transient structures (e.g. solar panels and radiators) and irregularly transient structures (e.g. robotic arms). Most GRBs detected by CGBM arrived from the direction not obstructed by the fixed structures. However, some GRBs arrived from the obstructed region. Although localization errors were ignored, there is $5 - 15$ deg uncertainty for each point. Also, there is a possibility that ISS structures might have gaps. Full effects of the ISS structures on CGBM data are unclear, and we continue to investigate this issues.

In the gamma-ray analysis with CAL, data collected in the high energy trigger (HE) mode and low energy gamma-ray (LEG) mode are used for the analysis above 10 GeV and 1 GeV, respectively [16]. The HE mode is the primary trigger mode of CAL. The HE mode is available anytime except when CAL is collecting pedestal data. LEG mode is enabled only at low latitude, or for a short

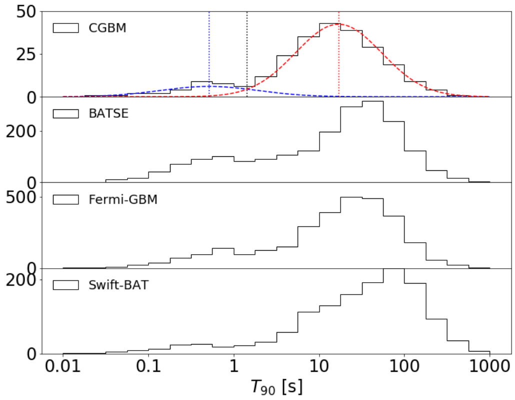

Figure 3: T_{90} distribution of CGBM GRBs. Energy ranges of CGBM, BATSE, *Fermi*-GBM, and *Swift*-BAT are 40 ~ 1000 keV, 25 ~ 2000 keV, 50 ~ 300 keV, and 15 ~ 350 keV, respectively [17–21]. Blue and red dashed lines are two optimized logarithmic normal distributions. Blue and red dotted lines show mean of the two distributions. Gray dotted line shows the intersection of the two distributions.

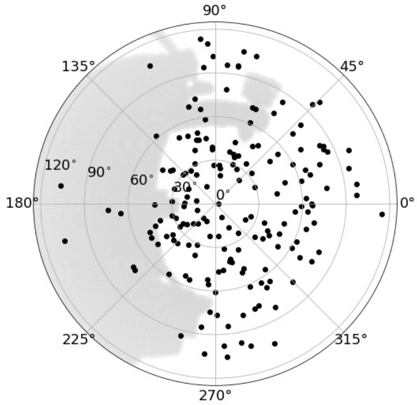

Figure 4: Incident angle distribution of GRBs in the SGM field of view. Black points are GRB positions in the SGM coordinate. A gray shaded region is the ISS fixed structure viewed from CALET.

period when a CGBM onboard trigger occurs [22]. We have continued to search for high-energy gamma-rays using CAL data [23]. We searched for high-energy gamma-rays from GRBs detected by CGBM using CAL data up to September 30 in 2020. We searched for gamma-ray events in 1 GeV ~ 10 GeV for 99 GRBs which were well localized by *Swift*-BAT, XRT, UVOT, *Fermi*-LAT, MAXI-GSC, and IPN, using LEG data from $T_0 - 60$ s to $T_0 + 7200$ s within 2 deg from the reported GRB central position, where T_0 is the trigger time of CGBM. The gamma-ray identification was performed according to the method described in [16]. The directions obstructed by fixed structures and moving structures except transient obstruction (e.g., robotic arms), were masked to exclude secondary gamma-rays from the structures. In the case of gamma-ray candidates from GRBs were found, we checked the effects of transient obstruction for each candidate by making scatter plots of arrival directions of gamma-ray candidates on the detector coordinate. As a result, the GRB positions were outside of the CAL field of view, or there was no available LEG data for 37 GRBs. There was no gamma-ray event near the GRB positions for 59 GRBs, even if the GRB positions were in the CAL field of view. Gamma-ray events were found near the position of GRB 180526A, GRB 200101A, and GRB 200613A. In the case of GRB 200613A, we found the robotic arm obstructed the CAL field of view on June 13, 2020, and we concluded the gamma-ray event was a secondary gamma-ray event from the obstructions. CGBM detected GRB 180526A at T_0 = 2018/05/26 11:03:36.20 UT. A 3.4 GeV gamma-ray event was found at 1.3 deg. away from the reported position (R.A., Dec.) = (108.48 deg., 3.64 deg.) by Fermi-LAT at T_0 + 244 s [24] . The central position of GRB 180526A was within the 99 % PSF region of the candidate. CGBM also detected GRB 200101A at T_0 = 2020/01/01 20:39:30.40 UT. A 4.9 GeV gamma-ray event was found at 0.6 deg. away from the reported position (R.A., Dec.) = (258.995 deg., −32.304 deg.) by IPN at T_0 + 105 s [15] (#26635). The central position of GRB 200101A was within the 90 % PSF region

Table 2: Summary of follow-up observation for gravitational wave events in O3

Event name	Possible source	Event time (T_0)	CGBM trigger	P_h	P_{cal}	Run mode	90 % Upper limit [erg s^{-1} cm^{-2}]	GCN Circular#
S190408an	BBH (>99 %)	2019/04/08 18:18:02.288180	No trigger	96 %	80 %	LEG	2.3×10^{-6}	24088
S190412m	BBH (>99 %)	2019/04/12 05:30:44.165622	Disabled	-	-	-	-	-
S190421ar	BBH (97 %)	2019/04/21 21:38:56.250977	No trigger	3 %	0 %	-	-	-
S190425z	BNS (>99 %)	2019/04/25 08:18:05.017147	Disabled	-	5 %	HE	1.0×10^{-4}	24218
S190426c	BNS (49 %)	2019/04/26 15:21:55.336540	Disabled	-	10 %	HE	2.5×10^{-5}	24276
S190503bf	BBH (96 %)	2019/05/03 18:54:04.294490	Disabled	-	10 %	HE	4.2×10^{-5}	24403
S190510g	Terrestrial (58 %)	2019/05/10 02:59:39.291636	No trigger	16 %	0 %	-	-	24495
S190512at	BBH (99 %)	2019/05/12 18:07:14.422363	No trigger	100 %	10 %	HE	1.9×10^{-5}	24531
S190513bm	BBH (94 %)	2019/05/13 20:54:28.747089	No trigger	100 %	5 %	LEG	6.0×10^{-5}	24548
S190517h	BBH (98 %)	2019/05/17 05:51:01.830582	No trigger	89 %	0 %	-	-	24593
S190519bj	BBH (96 %)	2019/05/19 15:35:44.397949	No trigger	100 %	0 %	-	-	24617
S190521g	BBH (97 %)	2019/05/21 03:02:29.447266	Disabled	-	30 %	HE	6.0×10^{-6}	24648
S190521r	BBH (>99 %)	2019/05/21 07:43:59.463379	Disabled	-	0 %	-	-	24649
S190602aq	BBH (99 %)	2019/06/02 17:59:27.089355	No trigger	99 %	5 %	HE	2.9×10^{-4}	24735
S190630ag	BBH (94 %)	2019/06/30 18:52:05.179550	Disabled	-	25 %	HE	1.2×10^{-5}	24960
S190701ah	BBH (93 %)	2019/07/01 20:33:06.577637	No trigger	30 %	0 %	-	-	24970
S190706ai	BBH (99 %)	2019/07/06 22:26:41.344727	Disabled	-	0 %	-	-	25027
S190707q	BBH (>99 %)	2019/07/07 09:33:26.181226	No trigger	76 %	20 %	LEG	2.1×10^{-6}	25033
S190718y	Terrestrial (98 %)	2019/07/18 14:35:12.067865	No trigger	22 %	5 %	LEG	1.7×10^{-6}	25099
S190720a	BBH (99 %)	2019/07/20 00:08:36.704102	Disabled	-	25 %	HE	3.0×10^{-5}	25134
S190727h	BBH (92 %)	2019/07/27 06:03:33.985887	No trigger	35 %	0 %	-	-	25184
S190728q	MassGap (52 %)	2019/07/28 06:45:10.529205	No trigger	0 %	0 %	-	-	25214
S190814bv	NSBH (>99 %)	2019/08/14 21:10:39.012957	Disabled	-	0 %	-	-	25390
Fermi GBM-190816	sub-threshold	2019/08/16 21:22:13.027	No trigger	66 %	25 %	HE	2.1×10^{-4}	-
S190828j	BBH (>99 %)	2019/08/28 06:34:05.756472	No trigger	42 %	0 %	-	-	25536
S190828l	BBH (>99 %)	2019/08/28 06:55:09.886557	No trigger	79 %	0 %	-	-	25537
S190901ap	BNS (86 %)	2019/09/01 23:31:01.837767	Disabled	82 %	5 %	LEG	6.3×10^{-5}	25647
S190910d	NSBH (98 %)	2019/09/10 01:26:19.242676	No trigger	77 %	0 %	-	-	25734
S190910h	BNS (61 %)	2019/09/10 08:29:58.544448	No trigger	75 %	10 %	LEG	9.4×10^{-6}	25735
S190915ak	BBH (99 %)	2019/09/15 23:57:02.690891	No trigger	100 %	0 %	-	-	25770
S190923y	NSBH (68 %)	2019/09/23 12:55:59.645508	No trigger	68 %	10 %	HE	1.2×10^{-5}	25830
S190924h	MassGap (> 99 %)	2019/09/24 02:18:46.846654	Disabled	-	0 %	-	-	25844
S190930s	MassGap (95 %)	2019/09/30 13:35:41.246810	No trigger	100 %	5 %	HE	3.5×10^{-5}	25891
S190930t	NSBH (74 %)	2019/09/30 14:34:07.685342	No trigger	74 %	5 %	HE	1.7×10^{-5}	25892
S191105e	BBH (95 %)	2019/11/05 14:35:21.933105	Disabled	-	0 %	-	-	26195
S191109d	BBH (>99 %)	2019/11/09 01:07:17.220703	Disabled	-	0 %	-	-	26236
S191129u	BBH (>99 %)	2019/11/29 13:40:29.197372	No trigger	68 %	0%	-	-	26321
S191204r	BBH (>99 %)	2019/12/04 17:15:26.091822	No trigger	4 %	0 %	-	-	26358
S191205ah	NSBH (93 %)	2019/12/05 21:52:08.568738	Disabled	-	0%	-	-	26377
S191213g	BNS (77 %)	2019/12/13 04:34:08.142224	No trigger	33 %	0 %	-	-	26419
S191215w	BBH (>99 %)	2019/12/15 22:30:52.333152	No trigger	51 %	0 %	-	-	26465
S191216ap	BBH (99 %)	2019/12/16 21:33:38.472999	No trigger	26 %	0 %	-	-	26481
S191222n	BBH (>99 %)	2019/12/22 03:35:37.119478	No trigger	60 %	0 %	-	-	26602
S200105ae	Terrestrial (97 %)	2020/01/05 16:24:26.057208	No trigger	84 %	60 %	HE	6.5×10^{-6}	26664
S200112r	BBH (>99 %)	2020/01/12 15:58:38.093931	No trigger	70 %	5 %	HE	1.1×10^{-6}	26740
S200114f	-	2020/01/14 02:08:18.239300	Disabled	-	80 %	HE	4.7×10^{-6}	26761
S200115j	MassGap (>99 %)	2020/01/15 04:23:09.742047	Disabled	-	20 %	HE	1.7×10^{-6}	26797
S200128d	BBH (97 %)	2020/01/28 02:20:11.903320	No trigger	65 %	10 %	HE	4.6×10^{-6}	26924
S200129m	BBH (>99 %)	2020/01/29 06:54:58.435104	Disabled	-	5 %	HE	5.7×10^{-5}	26941
S200208q	BBH (>99 %)	2020/02/08 13:01:17.991118	Disabled	-	0 %	-	-	27030
S200213t	BNS (63 %)	2020/02/13 04:10:40.327981	No trigger	31 %	0 %	-	-	27084
S200219ac	BBH (96 %)	2020/02/19 09:44:15.195312	No trigger	73 %	0 %	-	-	27149
S200224ca	BBH (>99 %)	2020/02/24 22:22:34.405762	Disabled	-	95 %	HE	5.0×10^{-7}	27231
S200225q	BBH (96 %)	2020/02/25 06:04:21.396973	Disabled	-	0 %	-	-	27232
S200302c	BBH (89 %)	2020/03/02 01:58:11.519119	No trigger	81 %	0 %	-	-	27299
S200311bg	BBH (>99 %)	2020/03/11 11:58:53.397788	Disabled	-	0 %	-	-	27372
S200316bj	MassGap (>99 %)	2020/03/16 21:57:56.157221	No trigger	82 %	35 %	HE	2.8×10^{-6}	27405

of the candidate. No excess can be seen in CGBM at the arrival time of the candidates for GRB 180526A and GRB 200101A. A detailed analysis is still underway.

3. Follow-up for gravitational wave events in LIGO/Virgo O3

CALET participated in the follow-up campaign for the LIGO/Virgo first and second observation runs [25][26][6]. Also, we performed a follow-up observation of electromagnetic counterparts of the gravitational wave using both CAL and CGBM data in the LIGO/Virgo third observation run

(O3) [27] [11]. Table 2 shows a summary of CALET follow-up observations. There are 56 events reported by the LIGO/Virgo collaboration (LVC) and one sub-threshold event reported by LVC and *Fermi*-GBM team[28] [15]. 'Event name,' 'Possible source,' and 'Event time (T_0)' are based on GraceDB and GCN circulars reported by the LVC and Fermi-GBM team [28][15](#25406). The 'Possible source' column shows just the highest probability source in the GCN circulars.

'CGBM trigger' shows the status of the CGBM onboard trigger at T_0. 'No trigger' means that CGBM onboard trigger was enabled; however, no trigger occurred in T_0-60 s~ T_0+ 60 s. 'Disabled' means the CGBM onboard trigger was disabled due to CGBM high voltages were off, or the CGBM event data storage was full. There were no onboard triggers associated with any gravitational wave events. 'P_h' shows the summed LIGO/Virgo localization probability above the horizon. If the CGBM high voltages were off, the column was filled by '-.' We also searched for electromagnetic signals in TH data for 36 events that occurred when the CGBM high voltage was on. We calculated the SNRs using (1) with extended conditions and searched for significant signals according to the method described in [11] using TH data for T_0-60 s~ T_0+ 60 s, where T_0 is the trigger time of the gravitational wave event. As a result, there was no significant signal associated with the gravitational wave events in the CGBM data.

'P_{cal}' shows the summed LIGO/Virgo localization probability in the CAL field of view for T_0-60 s~ T_0+ 60 s. Although CAL's high voltages are typically always on, CALET was off due to a special activity on ISS when S190412 occurred. 'Run mode' shows the CAL run mode at T_0. If P_{cal} is zero, the column was filled by '-.' In the case where P_{cal} was 5 % or greater, we searched for gamma-ray events from the LIGO/Virgo localization high probability region in HE (10 GeV ~ 100 GeV) or LEG (1 GeV ~ 10 GeV) data for T_0-60 s~ T_0+ 60 s. Although there was no high energy gamma-ray candidate associated with the gravitational wave events, we estimated 90 % upper limits of gamma-ray flux for each direction according to the method described in [26][27]. The 90 % upper limits were calculated for the energy range 10 GeV ~ 100 GeV and 1 GeV ~ 10 GeV in the case of HE and LEG data, respectively. As examples of the analysis, Figure 5 shows the 90% upper limits maps for S190408an and S200316bj. Since effective areas for small incident angles are larger than that for large incident angles, stricter upper limits are derived near the CALET zenith than near the edge of the CAL field of view. The dented structures around the edge of the CAL field of view were masked due to the fixed ISS structures. '90 % Upper limit ' shows the highest 90 % upper limits of gamma-ray flux when the summed LIGO/Virgo localization probability reached P_{cal}.

4. Summary

CALET has been in in-orbit operation since October 2015 without any problems. CGBM has been continuing all-sky monitoring of GRBs with a ~60 % duty cycle and observed 254 GRBs, including 31 short GRBs, by the end of May 2021. As the result of high energy gamma-ray search from GRBs detected by CGBM using CAL, two gamma-ray candidates were found from GRB 180526A and GRB 200101A. CALET also participated in the follow-up campaign for electromagnetic counterparts of gravitational wave events in O3. Although there was no candidate of the electromagnetic counterparts, we estimated 90 % upper limits of gamma-ray flux for 26 gravitational wave events using CAL data.

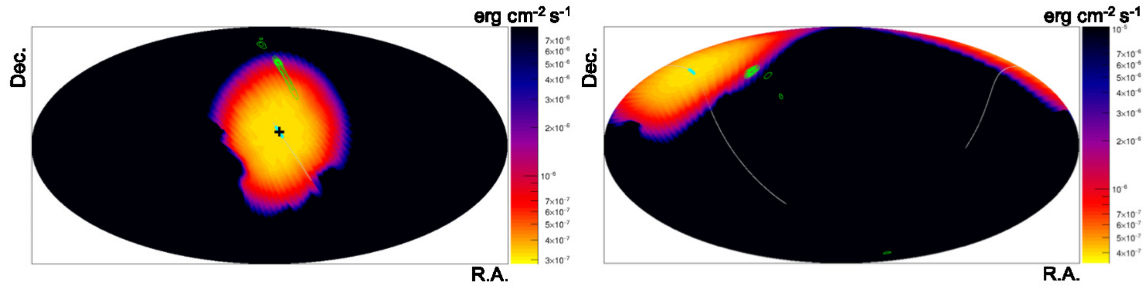

Figure 5: The 90 % upper limits for S190408an (left) and S200316bj (right). The color maps show the 90 % upper limits of gamma-ray flux. In the case of S190408A, the energy range is 1 GeV ∼ 10 GeV. In the case of S200316bj, energy range is 10 GeV ∼ 100 GeV. Green contours are the LIGO/Virgo localization high probability region. Black bold cross is the CAL zenith at T_0. Cyan bold lines are tracks of the CAL zenith for T_0-60 s∼ T_0+ 60 s.

References

[1] R. Y. Klebesadel et al., *OBSERVATIONS OF GAMMA-RAY BURSTS OF COSMIC ORIGIN*, *THE ASTROPHYSICAL JOURNAL*, **182**, L85, (1973)

[2] P. Kumar, and B. Zhang, *The physics of gamma-ray bursts & relativistic jets*, *Physics Report*, **561**, 1, (2015).

[3] C. Kouveliotou et al., *IDENTIFICATION OF TWO CLASSES OF GAMMA-RAY BURSTS*, *THE ASTROPHYSICAL JOURNAL*, **413**, L101, (1993).

[4] B. P. Abbott et al., *GW170817: Observation of Gravitational Waves from a Binary Neutron Star Inspiral*, *PHYSICAL REVIEW LETTERS*, **119**, 161101, (2017).

[5] B. P. Abbott et al., *Gravitational Waves and Gamma-Rays from a Binary Neutron Star Merger: GW170817 and GRB 170817A*, *THE ASTROPHYSICAL JOURNAL LETTERS*, **848**, L13, (2017).

[6] B. P. Abbott et al., *Multi-messenger Observations of a Binary Neutron Star Merger*, *The Astrophysical Journal Letters*, **848**, L12, (2017).

[7] Y Asaoka for the CALET Collaboration, *The CALorimetric Electron Telescope (CALET) on the International Space Station*, *Proc.36th ICRC (Madison, USA, 2019)*, POS(ICRC2019), 001, (2019).

[8] N. Cannady on behalf of the CALET Collaboration, *Low-energy gamma-ray observations above 1 GeV with CALET on the International Space Station*, in this conference.

[9] M. Mori on behalf of the CALET Collaboration., *High-energy gamma-ray observations above 10 GeV with CALET on the International Space Station*, in this conference.

[10] K. Yamaoka et al., *The CALET Gamma-ray Burst Monitor (CGBM)) Proc. 7th Huntsville Gamma-Ray Burst Symposium (Nashville, USA, 2013)*, paper 41 in eConf Proceedings C1304143, (2013).

[11] Y. Kawakubo et al., *Search for electromagnetic counterparts of gravitational wave sources with CALET*, *Proc. GAMMA-RAY BURSTS IN THE GRAVITATIONAL WAVE ERA*, 31, (2020).

[12] F.G.A. Quarati et al., *Study of ^{138}La radioactive decays using LaBr$_3$ scintillators*, *Nuclear Instruments and Methods in Physics Research A*, **683**, 46, (2012)

[13] P.R. Truscott et al., *Activation of Space-Borne Bismuth Germanate γ-ray Detectors*, *IEEE TRANSACTIONS ON NUCLEAR SCIENCE*, **42**, No.4, (1995)

[14] NASA HEASARC battblocks `https://heasarc.gsfc.nasa.gov/ftools/caldb/help/battblocks.html`

[15] The Gamma-ray Coordinates Network `https://gcn.gsfc.nasa.gov`

[16] N. Cannady et al., *Characteristics and Performance of the CALorimetric Electron Telescope (CALET) Calorimeter for Gamma-Ray Observations*, *The Astrophysical Journal Supplement Series*, **238**, 5, (2018)

[17] D. Gruber et al., *THE FERMI GBM GAMMA-RAY BURST SPECTRAL CATALOG: FOUR YEARS OF DATA*, *THE ASTROPHYSICAL JOURNAL SUPPLEMENT SERIES*, **211**, 12, (2014).

[18] A. von Kienlin et al., *THE SECOND FERMI GBM GAMMA-RAY BURST CATALOG: THE FIRST FOUR YEARS*, *THE ASTROPHYSICAL JOURNAL SUPPLEMENT SERIES*, **211**, 13, (2014).

[19] P. N. Bhat et al., *THE THIRD FERMI GBM GAMMA-RAY BURST CATALOG: THE FIRST SIX YEARS*, *THE ASTROPHYSICAL JOURNAL SUPPLEMENT SERIES*, **223**, 28, (2016).

[20] The BATSE Current Gamma-Ray Burst Catalog, the BATSE GRB Team, `https://gammaray.msfc.nasa.gov/batse/grb/catalog/current/`

[21] The *Swift*/BAT Gamma-Ray Burst Catalog, `https://swift.gsfc.nasa.gov/results/batgrbcat/`

[22] Y. Asaoka et al., *On-orbit operations and offline data processing of CALET onboard the ISS*, *Astroparticle Physics*, **100**, 29, (2018).

[23] N. Cannady for the CALET collaboration, *CALET upper limits on GeV-energy gamma-ray burst emission*, *Proc.36th ICRC (Madison, USA, 2019)*, POS(ICRC2019), 557, (2019).

[24] Ajello, et al., *A Decade of Gamma-Ray Bursts Observed by Fermi-LAT: The Second GRB Catalog*, *The Astrophysical Journal*, **878**, 52, (2019).

[25] O. Adriani et al., *CALET UPPER LIMITS ON X-RAY AND GAMMA-RAY COUNTERPARTS OF GW151226*, *The Astrophysical Journal Letters*, **829**, L20, (2016).

[26] O. Adriani et al., *Search for GeV Gamma-Ray Counterparts of Gravitational Wave Events by CALET*, *The Astrophysical Journal*, **863**, 160, (2018).

[27] M. Mori & Y. Asaoka for the CALET Collaboration, *High-Energy Gamma-ray Observations Using the CALorimetric Electron Telescope (CALET) on the ISS*, *Proc.36th ICRC (Madison, USA, 2019)*, POS(ICRC2019), 586, (2019).

[28] GraceDB, `https://gracedb.ligo.org/superevents/public/O3/`

Full Authors List: CALET Collaboration

O. Adriani[1,2], Y. Akaike[3,4], K. Asano[5], Y. Asaoka[5], E. Berti[1,2], G. Bigongiari[6,7], W. R. Binns[8], M. Bongi[1,2], P. Brogi[6,7], A. Bruno[9,10], J. H. Buckley[8], N. Cannady[11,12,13], G. Castellini[14], C. Checchia[6], M. L. Cherry[15], G. Collazuol[16,17], K. Ebisawa[18], A. W. Ficklin[15], H. Fuke[18], S. Gonzi[1,2], T. G. Guzik[15], T. Hams[11], K. Hibino[19], M. Ichimura[20], K. Ioka[21], W. Ishizaki[5], M. H. Israel[8], K. Kasahara[22], J. Kataoka[23], R. Kataoka[24], Y. Katayose[25], C. Kato[26], N. Kawanaka[27,28], Y. Kawakubo[15], K. Kobayashi[3,4], K. Kohri[29], H. S. Krawczynski[8], J. F. Krizmanic[11,12,13], P. Maestro[6,7], P. S. Marrocchesi[6,7], A. M. Messineo[30,7], J.W. Mitchell[12], S. Miyake[32], A. A. Moiseev[33,12,13], M. Mori[34], N. Mori[2], H. M. Motz[35], K. Munakata[26], S. Nakahira[18], J. Nishimura[18], G. A. de Nolfo[9], S. Okuno[19], J. F. Ormes[36], N. Ospina[16,17], S. Ozawa[37], L. Pacini[1,14,2], P. Papini[2], B. F. Rauch[8], S. B. Ricciarini[14,2], K. Sakai[11,12,13], T. Sakamoto[38], M. Sasaki[33,12,13], Y. Shimizu[19], A. Shiomi[39], P. Spillantini[1], F. Stolzi[6,7], S. Sugita[38], A. Sulaj[6,7], M. Takita[5], T. Tamura[19], T. Terasawa[40], S. Torii[3], Y. Tsunesada[41], Y. Uchihori[42], E. Vannuccini[2], J. P. Wefel[15], K. Yamaoka[43], S. Yanagita[44], A. Yoshida[38], K. Yoshida[22], and W. V. Zober[8]

[1]Department of Physics, University of Florence, Via Sansone, 1, 50019 Sesto, Fiorentino, Italy, [2]INFN Sezione di Florence, Via Sansone, 1, 50019 Sesto, Fiorentino, Italy, [3]Waseda Research Institute for Science and Engineering, Waseda University, 17 Kikuicho, Shinjuku, Tokyo 162-0044, Japan, [4]JEM Utilization Center, Human Spaceflight Technology Directorate, Japan Aerospace Exploration Agency, 2-1-1 Sengen, Tsukuba, Ibaraki 305-8505, Japan, [5]Institute for Cosmic Ray Research, The University of Tokyo, 5-1-5 Kashiwa-no-Ha, Kashiwa, Chiba 277-8582, Japan, [6]Department of Physical Sciences, Earth and Environment, University of Siena, via Roma 56, 53100 Siena, Italy, [7]INFN Sezione di Pisa, Polo Fibonacci, Largo B. Pontecorvo, 3, 56127 Pisa, Italy, [8]Department of Physics and McDonnell Center for the Space Sciences, Washington University, One Brookings Drive, St. Louis, Missouri 63130-4899, USA, [9]Heliospheric Physics Laboratory, NASA/GSFC, Greenbelt, Maryland 20771, USA, [10]Department of Physics, Catholic University of America, Washington, DC 20064, USA, [11]Center for Space Sciences and Technology, University of Maryland, Baltimore County, 1000 Hilltop Circle, Baltimore, Maryland 21250, USA, [12]Astroparticle Physics Laboratory, NASA/GSFC, Greenbelt, Maryland 20771, USA, [13]Center for Research and Exploration in Space Sciences and Technology, NASA/GSFC, Greenbelt, Maryland 20771, USA, [14]Institute of Applied Physics (IFAC), National Research Council (CNR), Via Madonna del Piano, 10, 50019 Sesto, Fiorentino, Italy, [15]Department of Physics and Astronomy, Louisiana State University, 202 Nicholson Hall, Baton Rouge, Louisiana 70803, USA, [16]Department of Physics and Astronomy, University of Padova, Via Marzolo, 8, 35131 Padova, Italy, [17]INFN Sezione di Padova, Via Marzolo, 8, 35131 Padova, Italy, [18]Institute of Space and Astronautical Science, Japan Aerospace Exploration Agency, 3-1-1 Yoshinodai, Chuo, Sagamihara, Kanagawa 252-5210, Japan, [19]Kanagawa University, 3-27-1 Rokkakubashi, Kanagawa, Yokohama, Kanagawa 221-8686, Japan, [20]Faculty of Science and Technology, Graduate School of Science and Technology,, Hirosaki University, 3, Bunkyo, Hirosaki, Aomori 036-8561, Japan, [21]Yukawa Institute for Theoretical Physics, Kyoto University, Kitashirakawa Oiwakecho, Sakyo, Kyoto 606-8502, Japan, [22]Department of Electronic Information Systems, Shibaura Institute of Technology, 307 Fukasaku, Minuma, Saitama 337-8570, Japan, [23]School of Advanced Science and Engineering, Waseda University, 3-4-1 Okubo, Shinjuku, Tokyo 169-8555, Japan, [24]National Institute of Polar Research, 10-3, Midori-cho, Tachikawa, Tokyo 190-8518, Japan, [25]Faculty of Engineering, Division of Intelligent Systems Engineering, Yokohama National University, 79-5 Tokiwadai, Hodogaya, Yokohama 240-8501, Japan, [26]Faculty of Science, Shinshu University, 3-1-1 Asahi, Matsumoto, Nagano 390-8621, Japan, [27]Hakubi Center, Kyoto University, Yoshida Honmachi, Sakyo-ku, Kyoto 606-8501, Japan, [28]Department of Astronomy, Graduate School of Science, Kyoto University, Kitashirakawa Oiwake-cho, Sakyo-ku, Kyoto 606-8502, Japan, [29]Institute of Particle and Nuclear Studies, High Energy Accelerator Research Organization, 1-1 Oho, Tsukuba, Ibaraki 305-0801, Japan, [30]University of Pisa, Polo Fibonacci, Largo B. Pontecorvo, 3, 56127 Pisa, Italy, [31]Astroparticle Physics Laboratory, NASA/GSFC, Greenbelt, Maryland 20771, USA, [32]Department of Electrical and Electronic Systems Engineering, National Institute of Technology, Ibaraki College, 866 Nakane, Hitachinaka, Ibaraki 312-8508, Japan [33]Department of Astronomy, University of Maryland, College Park, Maryland 20742, USA, [34]Department of Physical Sciences, College of Science and Engineering, Ritsumeikan University, Shiga 525-8577, Japan, [35]Faculty of Science and Engineering, Global Center for Science and Engineering, Waseda University, 3-4-1 Okubo, Shinjuku, Tokyo 169-8555, Japan, [36]Department of Physics and Astronomy, University of Denver, Physics Building, Room 211, 2112 East Wesley Avenue, Denver, Colorado 80208-6900, USA, [37]Quantum ICT Advanced Development Center, National Institute of Information and Communications Technology, 4-2-1 Nukui-Kitamachi, Koganei, Tokyo 184-8795, Japan, [38]College of Science and Engineering, Department of Physics and Mathematics, Aoyama Gakuin University, 5-10-1 Fuchinobe, Chuo, Sagamihara, Kanagawa 252-5258, Japan, [39]College of Industrial Technology, Nihon University, 1-2-1 Izumi, Narashino, Chiba 275-8575, Japan [40]RIKEN, 2-1 Hirosawa, Wako, Saitama 351-0198, Japan, [41]Division of Mathematics and Physics, Graduate School of Science, Osaka City University, 3-3-138 Sugimoto, Sumiyoshi, Osaka 558-8585, Japan, [42]National Institutes for Quantum and Radiation Science and Technology, 4-9-1 Anagawa, Inage, Chiba 263-8555, Japan, [43]Nagoya University, Furo, Chikusa, Nagoya 464-8601, Japan, [44]College of Science, Ibaraki University, 2-1-1 Bunkyo, Mito, Ibaraki 310-8512, Japan